UC San Diego
UC San Diego Previously Published Works

Title
Isolated broadband attosecond pulse generation with near- and mid-infrared driver pulses via time-gated phase matching.

Permalink

Journal

ISSN

Authors
Hernández-García, C
Popmintchev, T
Murnane, MM
et al.

Publication Date

DOI

Peer reviewed

Isolated broadband attosecond pulse generation with near- and mid-infrared driver pulses via time-gated phase matching

C. Hernández-García,[1,2,*] T. Popmintchev,[3] M. M. Murnane,[1] H. C. Kapteyn,[1] L. Plaja,[2] A. Becker,[1] and A. Jaron-Becker[1]

[1]*JILA and Department of Physics, University of Colorado at Boulder, Boulder, CO 80309-0440, USA*
[2]*Grupo de Investigación en Aplicaciones del Láser y Fotónica, Departamento de Física Aplicada, University of Salamanca, E-37008, Salamanca, Spain*
[3]*Department of Physics and Center for Advanced Nanoscience, University of California San Diego, La Jolla, CA 92093, USA*
*carloshergar@usal.es

Abstract: We present a theoretical analysis of the time-gated phase matching (ionization gating) mechanism in high-order harmonic generation for the isolation of attosecond pulses at near-infrared and mid-infrared driver wavelengths, for both few-cycle and multi-cycle driving laser pulses. Results of our high harmonic generation and three-dimensional propagation simulations show that broadband isolated pulses spanning from the extreme-ultraviolet well into the soft X-ray region of the spectrum can be generated for both few-cycle and multi-cycle laser pulses. We demonstrate the key role of absorption and group velocity matching for generating bright, isolated, attosecond pulses using long wavelength multi-cycle pulses. Finally, we show that this technique is robust against carrier-envelope phase and peak intensity variations.

References and links

1. A. McPherson, G. Gibson, H. Jara, U. Johann, T. S. Luk, I. A. McIntyre, K. Boyer, and C. K. Rhodes, "Studies of multiphoton production of vacuum-ultraviolet radiation in the rare gases," J. Opt. Soc. Am. B **4**, 595 (1987).
2. M. Ferray, A. L'Huillier, X.F. Li, L. A. Lompre, G. Mainfray and C. Manus, "Multiple-harmonic conversion of 1064 nm radiation in rare gases," J. Phys. B At. Mol. Opt. Phys. **21**, L31 (1988).
3. T. Popmintchev, M. Chen, D. Popmintchev, P. Arpin, S. Brown, S. Ališauskas, G. Andriukaitis, T. Balčiunas, O. Mücke, A. Pugzlys, A. Baltuška, B. Shim, S. E. Schrauth, A. Gaeta, C. Hernández-García, L. Plaja, A. Becker, A. Jaroń-Becker, M. M. Murnane, and H. C. Kapteyn, "Bright coherent ultrahigh harmonics in the keV X-ray regime from mid-infrared femtosecond lasers," Science **336**, 1287–1291 (2012).
4. K. J. Schafer, B. Yang, L. F. DiMauro, and K. C. Kulander, "Above threshold ionization beyond the high harmonic cutoff," Phys. Rev. Lett. **70**, 1599–1602 (1993).
5. P. B. Corkum, "Plasma perspective on strong-field multiphoton ionization," Phys. Rev. Lett. **71**, 1994–1997 (1993).
6. I. P. Christov, M. M. Murnane and H. C. Kapteyn, "High-harmonic generation of attosecond pulses in the 'single-cycle' regime," Phys. Rev. Lett. **78**, 1251–1254 (1997).
7. E. Goulielmakis, M. Schultze, M. Hofstetter, V. S. Yakovlev, J. Gagnon, M. Uiberacker, A. L. Aquila, E. M. Gullikson, D. T. Attwood, R. Kienberger, F. Krausz and U. Kleineberg, "Single-cycle nonlinear optics," Science **320**, 1614–1617 (2008).
8. I. J. Sola, E. Mével, L. Elouga, E. Constant, V. Strelkov, L. Poletto, P. Villoresi, E. Benedetti, J.-P. Caumes, S. Stagira, C. Vozzi, G. Sansone and M. Nisoli, "Controlling attosecond electron dynamics by phase-stabilized polarization gating," Nat. Phys. **2**, 319–322 (2006).
9. G. Sansone, E. Benedetti, F. Calegari, C. Vozzi, L. Avaldi, R. Flammini, L. Poletto, P. Villoresi, C. Altucci, R. Velotta, S. Stagira, S. De Silvestri, and M. Nisoli, "Isolated single-cycle attosecond pulses," Science **314**, 443–446 (2006).
10. E. J. Takahashi, P. Lan, O.D. Mücke, Y. Nabekawa, and K. Midorikawa, "Infrared two-color multicycle laser field synthesis for generating an intense attosecond pulse," Phys. Rev. Lett. **104**, 233901 (2010).
11. K. Zhao, Q. Zhang, M. Chini, Y. Wu, X. Wang, and Z. Chang, "Tailoring a 67 attosecond pulse through advantageous phase-mismatch," Opt. Lett. **37**, 3891–3893 (2012).
12. F. Ferrari, F. Calegari, M. Lucchini, C. Vozzi, S. Stagira, G. Sansone and M. Nisoli, "High-energy isolated attosecond pulses generated by above-saturation few-cycle fields," Nat. Photonics **4**, 875–879 (2010).

13. H. Mashiko, K. Oguri, and T. Sogawa, "Attosecond pulse generation in carbon K-edge region (284 eV) with sub-250 μJ driving laser using generalized double optical gating method," Appl. Phys. Lett. **102**, 171111 (2013).

14. M. Chini, K. Zhao, and Z. Chang, "The generation, characterization and applications of broadband isolated attosecond pulses," Nat. Photonics **8**, 178–186 (2014).

15. C. Hernández-García, C. G. Durfee, D. D. Hickstein, T. Popmintchev, A. Meier, M. M. Murnane, H. C. Kapteyn, I. J. Sola, A. Jaron-Becker, and A. Becker, "Schemes for generation of isolated attosecond pulses of pure circular polarization," Phys. Rev. A **93**, 043855 (2016).

16. E. Mevel, E. Constant, D. Garzella, P. Breger, C. Dorrer, C. Le Blanc, F. Salin, and P. Agostini, "Optimizing high order harmonic generation in absorbing gases," AIP Conf. Proc. **525**, 373 (2000).

17. S. Kazamias, D. Douillet, F. Weihe, C. Valentin, A. Rousse, S. Sebban, G. Grillon, F. Augé, D. Hulin, and Ph. Balcou, "Global optimization of high harmonic generation," Phys. Rev. Lett. **90**, 193901 (2003).

18. A. S. Sandhu, E. Gagnon, A. Paul, I. Thomann, A. Lytle, T. Keep, M. M. Murnane, H. C. Kapteyn, and I. P. Christov, "Generation of sub-optical-cycle, carrier-envelope-phase-insensitive, extreme-uv pulses via nonlinear stabilization in a waveguide," Phys. Rev. A, **74**, 061803R (2006).

19. V. V. Strelkov, E. Mével, and E. Constant, "Generation of isolated attosecond pulses by spatial shaping of a femtosecond laser beam," New J. Phys. **10**, 083040 (2008).

20. M. J. Abel, T. Pfeifer, P. M. Nagel, W. Boutu, M. J. Bell, C. P. Steiner, D. M. Neumark, and S. R. Leone, "Isolated attosecond pulses from ionization gating of high-harmonic emission," Chem. Phys. **366**, 9–14 (2009).

21. I. Thomann, A. Bahabad, X. Liu, R. Trebino, M. M. Murnane, and H. C. Kapteyn, "Characterizing isolated attosecond pulses from hollow-core waveguides using multi-cycle driving pulses," Opt. Express **17**, 4611–4633 (2009).

22. T. Popmintchev, M.C. Chen, A. Bahabad, M. Gerrity, P. Sidorenko, O. Cohen, I. P. Christov, M. M. Murnane, and H. C. Kapteyn, "Phase matching of high harmonic generation in the soft and hard X-ray regions of the spectrum," Proc. Natl. Acad. Sci. USA **106**, 10516–10521 (2009).

23. S. Kazamias, S. Daboussi, O. Guilbaud, K. Cassou, D. Ros, B. Cros, and G. Maynard, "Pressure-induced phase matching in high-order harmonic generation," Phys. Rev. A **83**, 063405 (2011).

24. M.-C. Chen, C. Mancuso, C. Hernández-García, F. Dollar, B. Galloway, D. Popmintchev, P. C. Huang, B. Walker, L. Plaja, A. A. Jaroń-Becker, A. Becker, M. M. Murnane, H. C. Kapteyn, and T. Popmintchev, "Generation of bright isolated attosecond soft X-ray pulses driven by multicycle midinfrared lasers," Proc. Natl. Acad. Sci. USA **111**, E2361–E2367 (2014).

25. H. Vincenti and F. Quéré, "Attosecond lighthouses: how to use spatiotemporally coupled light fields to generate isolated attosecond pulses," Phys. Rev. Lett. **108**, 113904 (2012).

26. F. Silva, S. M. Teichmann, S. L. Cousin, M. Hemmer, and J. Biegert, "Spatiotemporal isolation of attosecond soft X-ray pulses in the water window," Nat. Commun. **6**, 6611 (2015).

27. G. Andriukaitis, T. Balčiūnas, S. Ališauskas, A. Pugžlys, A. Baltuška, T. Popmintchev, M.-C. Chen, M. M. Murnane, and H. C. Kapteyn, "90 GW peak power few-cycle mid-infrared pulses from an optical parametric amplifier," Opt. Lett. **36**, 2755–2757 (2011).

28. I. Pupeza, D. Sánchez, J. Zhang, N. Lilienfein, M. Seidel, N. Karpowicz, T. Paasch-Colberg, I. Znakovskaya, M. Pescher, W. Schweinberger, V. Pervak, E. Fill, O. Pronin, Z. Wei, F. Krausz, A. Apolonski, abd J. Biegert, "High-power sub-two-cycle mid-infrared pulses at 100 MHz repetition rate," Nat. Photonics **9**, 721–724 (2015).

29. P. Salières, A. L'Huillier, and M. Lewenstein, "Coherence control of high-order harmonics," Phys. Rev. Lett. **74**, 3776–3779 (1995).

30. M. Bellini, C. Lynga, A. Tozzi, M. Gaarde, T. Hänsch, A. L'Huillier, and C. Wahlström, "Temporal coherence of ultrashort high-order harmonic pulses," Phys. Rev. Lett. **81**, 297–300 (1998).

31. M. B. Gaarde, F. Salin, E. Constant, Ph. Balcou, K. J. Schafer, K. C. Kulander, and A. L'Huillier, "Spatiotemporal separation of high harmonic radiation into two quantum path components," Phys. Rev. A **59**, 1367–1373 (1999).

32. C. Hernández-García and L. Plaja, "Off-axis compensation of attosecond pulse chirp," J. Phys. B **45**, 074021 (2012).

33. A. R. Rundquist, C. G. Durfee III, Z. Chang, C. Herne, S. Backus, M. M. Murnane, and H. C. Kapteyn, "Phase-matched generation of coherent soft X-rays," Science **280**, 1412–1415 (1998).

34. C. G. Durfee III, A. R. Rundquist, S. Backus, C. Herne, M. M. Murnane, and H. C. Kapteyn, "Phase matching of high-order harmonics in hollow waveguides," Phys. Rev. Lett. **83**, 2187–2190 (1999).

35. M. C. Chen, P. Arpin, T. Popmintchev, M. Gerrity, B. Zhang, M. Seaberg, M. M. Murnane and H. C. Kapteyn, "Bright, coherent, ultrafast soft X-ray harmonics spanning the water window from a tabletop light source," Phys. Rev. Lett. **105**, 173901 (2010).

36. M. V. Amosov, N. B. Delone, and V. P. Krainov, "Tunnel ionization of complex atoms and of atomic ions in an alternating electromagnetic field," Zh. Eksp. Teor. Fiz. **91**, 2008–2013 (1986).

37. C. Hernández-García, J. A. Pérez-Hernández, J. Ramos, E. Conejero Jarque, L. Roso, and L. Plaja, "High-order harmonic propagation in gases within the discrete dipole approximation," Phys. Rev. A **82**, 022432 (2010).

38. J.A. Pérez-Hernández, L. Roso, and L. Plaja, "Harmonic generation beyond the Strong-Field Approximation: the physics behind the short-wave-infrared scaling laws," Opt. Express **17**, 9891–9903 (2009).

39. L. V. Keldysh, "Ionization in the field of a strong electromagnetic wave," Zh. Eksp. Teor. Fiz. **47**, 1945–1957 (1964).

40. F. H. M. Faisal, "Multiple absorption of laser photons by atoms," J. Phys. B **6**, L89 (1973).

41. H. R. Reiss, "Effect of an intense electromagnetic field on a weakly bound system," Phys. Rev. A **22**, 1786 (1980).

42. C. Hernández-García, J.A. Pérez-Hernández, T. Popmintchev, M.M. Murnane, H.C. Kapteyn, A. Jaroń-Becker, A.

Becker, and L. Plaja, "Zeptosecond high harmonic keV X-ray waveforms driven by midinfrared laser pulses," Phys. Rev. Lett. **111**, 033002 (2013).

43. A. Becker and F. H. M. Faisal, "Intense-field many-body S-matrix theory," J. Phys. B **38**, R1–R56 (2005).
44. C. M. Heyl, H. Coudert-Alteirac, M. Miranda, M. Louisy, K. Kovacs, V. Tosa, E. Balogh, K. Varjú, A. L'Huillier, A. Couairon, and C. L. Arnold, "Scale-invariant nonlinear optics in gases," Optica **3**, 75–81 (2016).
45. W. Boutu, T. Auguste, O. Boyko, I. Sola, Ph. Balcou, L. Binazon, O. Gobert, H. Merdji, C. Valentin, E. Constant, E. Mével, and B. Carré, "High-order-harmonic generation in gas with a flat-top laser beam," Phys. Rev. A **84**, 063406 (2011).
46. C. Hernández-García and L. Plaja, "Resolving multiple rescatterings in high-order-harmonic generation," Phys. Rev. A **93**, 023402 (2016).
47. J. Bernhardt, P. T. Simard, W. Liu, H. L. Xu, F. Théberge, A. Azarm, J. F. Daigle, S. L. Chin, "Critical power for self-focussing of a femtosecond laser pulse in helium," Opt. Commun. **281**, 2248–2251 (2008).
48. E. Constant, D. Garzella, P. Breger, and E. Mével, "Optimizing high harmonic generation in absorbing gases: model and experiment," Phys. Rev. Lett. **82**, 1668–1671 (1999).
49. C. Hernández-García, I. J. Sola, and L. Plaja, "Signature of the transversal coherence length in high-order harmonic generation," Phys. Rev. A **88**, 043848 (2013).
50. C. Hernández-García, T. Popmintchev, M. M. Murnane, H. C. Kapteyn, L. Plaja, A. Becker, and A. Jaroń-Becker, "Group velocity matching in high-order harmonic generation driven by mid-infrared lasers," New J. Phys. **18**, 073031 (2016).
51. A. M. Weiner, "effect of group velocity mismatch on the measurement of ultrashort optical pulses via second harmonic generation," IEEE J. Quant. Electron, **19**, 1276–1283 (1983).
52. R. C. Eckardt and J. Reintjes, "Phase matching limitations of high efficiency second harmonic generation," IEEE J. Quant. Electron, **QE-20**, 1178–1187 (1984).
53. D. Popmintchev, C. Hernández-García, F. Dollar, C. Mancuso, J. A. Pérez-Hernández, M.-C. Chen, A. Hankla, X. Gao, B. Shim, A. L. Gaeta, M. Tarazkar, D. A. Romanov, R. J. Levis, J. A. Gaffney, M. Foord, S. B. Libby, A. Jaron-Becker, A. Becker, L. Plaja, M. M. Murnane, H. C. Kapteyn, and T. Popmintchev, "Ultraviolet surprise: Efficient soft x-ray high-harmonic generation in multiply ionized plasmas," Science **350**, 1225–1231 (2015).
54. D. J. Jones, S. A. Diddams, J. K. Ranka, A. Stentz, R. S. Windeler, J. L. Hall, S. T. Cundiff, "Carrier-envelope phase control of femtosecond mode-locked lasers and direct optical frequency synthesis," Science **288**, 635–639 (2000).
55. A. Baltuška, T. Fuji, and T. Kobayashi, "Controlling the carrier-envelope phase of ultrashort light pulses with optical parametric amplifiers," Phys. Rev. Lett. **88**, 133901 (2002).
56. M. Schultze, E. Goulielmakis, M. Uiberacker, M. Hofstetter, J. Kim, D. Kim, F. Krausz, and U. Kleineberg, "Powerful 170-attosecond XUV pulses generated with few-cycle laser pulses and broadband multilayer optics," New J. Phys. **9**, 243 (2007).

1. Introduction

High-order harmonic generation (HHG) in intense laser fields is a highly nonlinear process [1,2], in which light at the driver laser frequency is coherently upconverted to shorter wavelengths up to the soft X-ray regime [3]. Since high-order harmonics are generated during the rescattering and recombination of an electron wave packet with the residual ion [4,5], harmonic radiation is emitted in each half-cycle of the driver laser pulse. Therefore, the radiation is typically composed of a train of attosecond bursts, which is related to the number of times a rescattering process occurs in the driving laser pulse.

The ultrashort duration of the harmonic bursts makes it possible to capture dynamical processes of electrons and nuclei in atoms and molecules. For this goal it is sometimes preferable to generate or isolate a single attosecond burst of harmonic radiation. Over the last decade, different techniques have been proposed and developed to achieve this. Most of them rely on controlling the rescattering process on the microscopic (single atom) level, for example using few-cycle driver lasers [6,7], polarization gating [8,9], the combination of multicolor fields [10], double optical gating [11], or single-atom ionization gating with an intense electric field beyond the gas saturation intensity [12]. These methods have been mainly demonstrated using Ti:Sapphire laser pulses with a maximum harmonic photon energy of 284 eV in a single burst achieved to date [13,14]. Recently, it has been further proposed to apply some of these methods to isolate attosecond pulses of circular polarization [15].

A complementary approach for isolating a single attosecond burst from a train relies on macroscopic phase-matching. Methods based on isolation using macroscopic propagation ef-

fects include ionization gating or time-gated phase-matching [16–24] or spatio-temporal wave-front control [25, 26]. The time-gated phase-matching technique makes use of the compensation of the phase mismatch due to the free electrons and the neutral atoms in the laser focus. Since their relative contributions vary with the degree of ionization during the driving laser pulse, a finite temporal window of perfect matching can be achieved. This window can be reduced to a single laser half-cycle, leading to the desired phase-matched isolation of a single attosecond burst of harmonic radiation. This principle has been demonstrated in experiment and theory for the generation of 180 eV isolated attosecond pulses driven by 2 μm multi-cycle laser pulses recently [24]. The preferable use of long mid-infrared driving laser pulses for this technique, to-gether with the development of long wavelength laser systems [27, 28], presents an interesting route towards the generation of isolated high-energy attosecond pulses.

In this paper we perform a theoretical analysis based on three-dimensional HHG and prop-agation simulations to explore the limits of the time-gated phase-matching technique. To this end, we present in Section II a brief theoretical analysis of the technique along with an overview of the model used for the 3D propagation simulations. In Section III, we then show that isolated attosecond pulses in a broad range of energies, from the few-eV to the keV regime, can be generated by using near-infrared to mid-infrared driver wavelengths. We find that in contrast to certain other techniques in which cutoff harmonics are filtered to obtain an isolated pulse, the whole harmonic bandwidth is preserved. However, note that other techniques, such as polariza-tion gating [8, 9] or attosecond light house [25], can be applied to preserve the full bandwidth as well. Furthermore, we demonstrate that long wavelength multi-cycle driver laser pulses ex-hibit a better yield scaling of the isolated attosecond harmonic radiation than few-cycle pulses, which is due to the presence of group-velocity matching. Finally, we analyze the robustness of the technique with respect to variations of the carrier-to-envelope phase and the peak intensity of the driver pulse to show that this technique is robust against carrier-envelope phase and peak intensity variations.

2. Theory

In this section we first discuss and briefly analyze the ionization gating or time-gated phase matching mechanism using a one-dimensional longitudinal analytical model. In subsection 2.2 we outline the three-dimensional numerical method used to calculate the 3D full-quantum single-atom high harmonic spectra and the 3D propagation of the driving and harmonic fields. Note that the results presented in Section 3 are performed using this later method.

2.1. Time window for perfect phase matching

The time-gated phase-matching technique for isolating attosecond pulses has the advantage of operating in a macroscopic configuration where the effects of free electrons and neutral atoms in the refractive index of the fundamental beam are the dominant contributions to phase match-ing. This can be achieved for a (nearly) constant intensity profile along the propagation axis in a gas cell, a gas jet in a loose focusing geometry [24], or a waveguide [3, 22], where other contri-butions to phase matching such as the geometrical (Gouy phase) and the longitudinal variation of the intrinsic phase of the harmonics [29–32] are negligible. Under these assumptions, and considering a homogeneous gas target of length L and pressure P, the phase mismatch of the qth-order harmonic along the propagation direction (z) is given by [22, 33, 34]

$$\Delta k_q = k_q - \frac{\partial \phi_q}{\partial z} \simeq \Delta k_q^{free} + \Delta k_q^{neutrals} \simeq qP \left[\frac{\lambda e^2}{mc^2} \eta(t) - \frac{4\pi^2 \chi_0}{\lambda} [1 - \eta(t)] \right] \quad (1)$$

where ϕ_q is the phase of the qth-order harmonic, $\eta(t)$ is the time-dependent ionization, χ_0 is the linear susceptibility of the gas due to the neutral atoms, and m and e are the mass and charge of

the electron, respectively. The contributions from the free electrons and the neutrals to Δk_q are opposite in sign and therefore perfect phase matching ($\Delta k_q = 0$) can be achieved for an optimal ionized population η_{opt}, also called critical ionization. For a given pulse shape and duration, the condition for reaching η_{opt} near the peak of the pulse therefore corresponds to choosing the wavelength and peak intensity [22]. As a consequence, lower intensities are required to phase match harmonics driven by longer wavelengths. We note that in a waveguide geometry, an additional geometric term, that depends on the mode and on the waveguide radius (see e.g., Eq. (2) in Ref. [34], or Refs. [33, 35]) has to be taken into account and contributes to the phase mismatch, making it possible to use higher pressures and achieve higher harmonic yields, to compensate for low single-atom yield.

As mentioned above, due to the increase of the ionization (and a corresponding decrease of neutrals) over the laser pulse, perfect phase-matching can only be achieved during a finite temporal window $\Delta\tau$. This window is inversely proportional to the time derivative of the phase-mismatch function and scales with pressure and wavelength as

$$\frac{1}{\Delta\tau} \propto \frac{\partial \Delta k_q}{\partial \tau} L \simeq q P \lambda L \frac{\partial \eta(t)}{\partial \tau} \propto \lambda^n P L \tag{2}$$

where τ is in units of the laser period. To derive the final proportionality in Eq. (2) one should first note that under perfect phase-matching conditions (where the peak intensity is adjusted at each driving wavelength to reach η_{opt} at the center of the pulse) the harmonic order scales as $q \simeq \lambda^{2.7}$ [24]. On the other hand, using the ADK ionization rates [36], we have found that $\partial\eta(t)/\partial\tau \simeq \lambda^{-2}$ for the multi-cycle pulses used in the present calculations, leading to $n \simeq 1.7$. Note that the value for n varies slightly for other pulse lengths. Based on this analysis can therefore expect that the pressure-length product and the driving wavelength are the key parameters to modify the time window for perfect phase matching, and thus, to control the number of phase matched attosecond pulses after propagation.

2.2.   3D propagation simulations

To confirm these expectations, we have performed three-dimensional simulations including phase-matching of the high-order harmonics during propagation. We have computed harmonic propagation using the electromagnetic field propagator [37]. We discretize the target (gas cell or gas jet) into elementary radiators, and propagate the emitted field $\mathbf{E}_j(\mathbf{r}_j, t)$ to the far-field detector,

$$\mathbf{E}_j(\mathbf{r}_d, t) = \frac{q_j \mathbf{s}_d}{c^2 |\mathbf{r}_d - \mathbf{r}_j|} \times \left[\mathbf{s}_d \times \mathbf{a}_j \left(t - \frac{|\mathbf{r}_d - \mathbf{r}_j|}{c} \right) \right] \tag{3}$$

where $\mathbf{s}_d$ is the unitary vector pointing to the detector, and $\mathbf{r}_d$ and $\mathbf{r}_j$ are the position vectors of the detector and of the elementary radiator j, respectively. Due to the large excursion lengths of the electron wave packet at mid-infrared wavelengths, computation of the dipole acceleration of each elementary radiator via the exact solution of the time dependent Schrödinger equation (TDSE) would be time consuming. Instead, we have therefore used the SFA+ approach [38], an extension of the standard strong field approximation [39–41], which has been shown to provide results in good quantitative agreement with TDSE results for single-atom HHG yields from near to mid infrared [38, 42]. In Eq. (3) we assume that the harmonic radiation propagates with the vacuum phase velocity, which is a reasonable assumption for high-order harmonics. Finally, the total field at the detector has been computed as the coherent addition of the elementary contributions. Phase and group velocity propagation effects in the fundamental field are included through the contributions of the free charges and the neutrals to the time-dependent refractive index. The ionization rate $\eta(\mathbf{r}, t)$ has been computed via the quasi-static model of the ADK theory [36, 43], thus including nonlinear phase shifts in the driving field. Nonlinear spatial effects
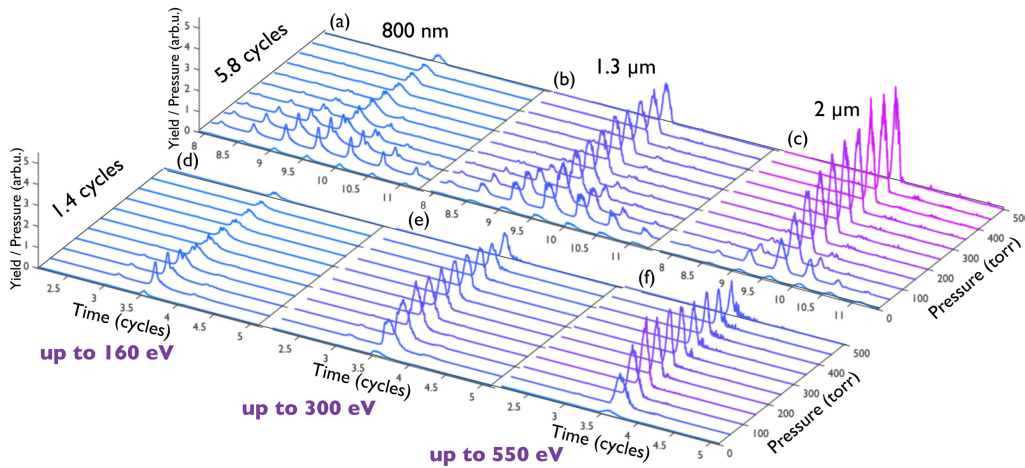
Fig. 1. Optimal gas pressure, laser wavelength and pulse duration for generating bright isolated attosecond pulses. We show the attosecond pulse yields and temporal profiles as a function of the gas pressure of a 2-mm-helium-gas-cell for driving laser pulses of wavelength (λ) 0.8 μm (a)(d), 1.3 μm (b)(e) and 2 μm (c)(f) and temporal duration (τ_p) of 1.4 (front row) and 5.8 (back row) cycles FWHM respectively. The laser pulse is modeled by a sin^2 envelope with a peak intensity chosen to match optimal phase matching conditions [22]. The yield in each lineout is divided by the gas pressure for the sake of clarity, and normalized to the yield of the attosecond pulse structure obtained at 5 torr.

are not taken into account. Absorption in the propagation of the harmonics is included through Beer's law.

In the results presented in this paper we have considered a loose focusing geometry. To this end, we have modeled our driving beam as a Bessel beam with a transverse field distribution given by $J_0(2.405\rho/a)$, where ρ is the radial coordinate, and $a = 60$ μm is the beam radius. Note that the main results obtained here are general and relevant to all other schemes where the driving beam longitudinal phase variation is negligible on the length scale of the target, such as a loosely focused Gaussian beam [44], a waveguide geometry [22, 33, 34], and flat-top beams [45, 46]. The driving beam propagates into a $L = 2$ mm helium cell centered at the beam focus. As an example of our results, we present the attosecond pulse emission detected on-axis. In our simulations we did not observe any relevant deviations for off-axis contributions of the XUV/soft x-ray beam. The driving laser field is of the form $sin^2(\pi t/2\sqrt{2}\tau_p)cos(2\pi ct/\lambda + \phi_{CEO})$, with wavelength λ, intensity pulse duration τ_p in full width at half maximum (FWHM) and carrier-envelope offset ϕ_{CEO}. In all simulations the peak intensity was chosen to match the optimal phase matching condition near the center of the pulse [22].

3. Results

In this section we use the results of our 3D numerical simulations to first demonstrate the isolation mechanism at different driver pulse wavelengths. We then proceed to analyze the role of group velocity matching and reabsorption for few- and multi-cycle laser pulses and, finally, consider variations of the pulse in the carrier envelope phase as well as the peak laser intensity.

3.1. Isolation of attosecond pulses at near-infrared to mid-infrared driver wavelengths

In figure 1 we present the variation of the attosecond pulse yield and temporal profile as a function of pressure at three different driving laser wavelengths (λ): 0.8 μm (a)(d), 1.3 μm (b)(e) and 2 μm (c)(f) and temporal durations (τ_p) of 1.4 (front row) and 5.8 (back row) cycles
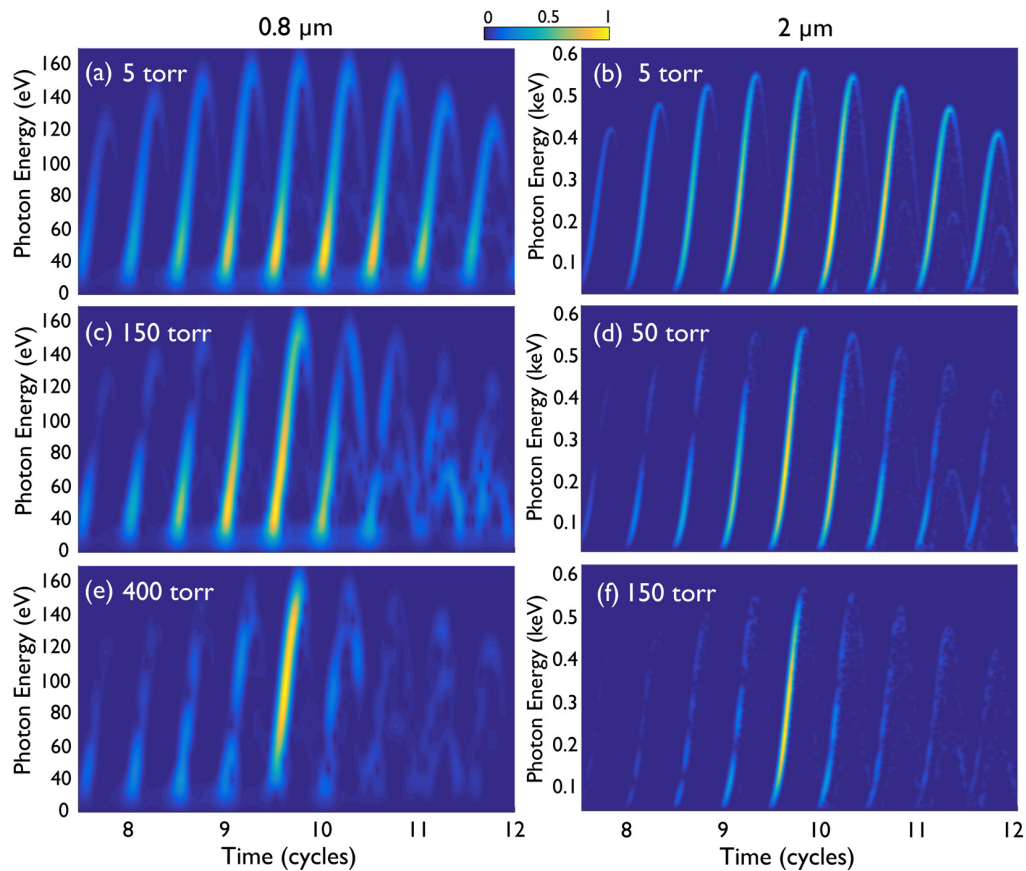
Fig. 2. Time gated phase-matching mechanism for the generation of soft X-ray isolated attosecond pulses. The time-frequency analysis of the high-harmonic radiation is shown for laser driving pulses of 0.8 μm (left column) and 2 μm (right column), and 5.8 cycles FWHM pulse duration. The pressure of the generating helium cell increases from (a) 5 torr to (e) 400 torr at 0.8 μm and from (b) 5 torr to (f) 150 torr at 2 μm. The time-frequency yield is normalized in each panel. Note that in agreement with theoretical prediction in Eq. (2), isolation of attosecond pulses occurs at lower pressures for the longer wavelength laser pulse.

at FWHM, respectively. The phase matched peak intensities for the 5.8 cycles (1.4 cycles) laser pulses are 6.76×10^{14} W/cm^2 (7.70×10^{14} W/cm^2) for 0.8 μm, 5.35×10^{14} W/cm^2 (6.01×10^{14} W/cm^2) for 1.3 μm, and 4.47×10^{14} W/cm^2 (4.96×10^{14} W/cm^2) for 2 μm. The carrier-envelope offset was set to $\phi_{CEO} = 0$ for the 5.8-cycle drivers and $\phi_{CEO} = 0.25\pi$ for the 1.4-cycle drivers to optimize the isolation of a single attosecond pulse. The yield in each panel is normalized to the yield of the attosecond pulse structure obtained at 5 torr. In order to show a clear comparison of the growth of the attosecond pulse yield with pressure, we have also divided the attosecond pulse yield by the gas pressure (i.e., the yield must be multiplied by the pressure to obtain the actual scaling, as performed later on in Section 3.2).

For the 1.4-cycle drivers presented in Figs. 1(d) to (f), we observe that isolated attosecond pulses are already obtained at lower pressures, but the scaling of their yield with pressure varies with the driving wavelength. For the results using 5.8-cycle drivers, presented in Figs. 1(a) to (c), we observe the trends predicted by Eq. (2). First, in each panel, as the pressure is increased, the

number of pulses in the train is reduced towards the isolation of a single attosecond burst of 360 as at 0.8 μm, 555 as at 1.3 μm and 650 as at 2 μm. Second, the longer the driver wavelength is, the lower is the pressure needed to isolate a single burst. As a consequence time-gated isolation of attosecond pulses driven by long-wavelength lasers also mitigates nonlinear effects, which typically appear at high pressures. Note that for the pressures considered in this work (<1 atm), nonlinear effects in helium are negligible [47]. We expect that the scaling of the attosecond pulse yields would be modified if pressures >1 atm are used.

In order to get more insight into the isolation process, we compare in figure 2 the time-frequency analysis driven by 5.8-cycle pulses of 0.8 μm and 2 μm central wavelength for three helium pressures. The positive slope of the resulting structures indicates that the so-called *short* trajectories are dominant and, thus, the isolated attosecond pulses are positively chirped. Further, it can be observed how the phase matching window decreases as the pressure increases, reducing the harmonic yield in the wings of the train while preserving the whole harmonic bandwidth in the central cycle of the pulse during the process. This is in contrast to certain other techniques in which the selection of the cutoff harmonics is used to obtain an isolated attosecond pulse. According to the present results, the isolated attosecond pulses contain a true supercontinuum extending from a few-eV to 160 eV for the 0.8 μm driver pulse, and reaching 350 eV for 1.3 μm, and 0.55 keV for 2.0 μm laser pulses. Indeed, the present set of calculations do not indicate a limitation in the process and we may therefore expect that a few keV isolated attosecond pulses can be generated via the time-gated phase matching technique when driving high-order harmonics with even longer wavelengths [3].

3.2. Few-cycle vs. multi-cycle pulses

Next, we investigate in Fig. 3 the integrated yield of the central pulse of the train as a function of the gas pressure for the (a) multi-cycle (5.8 cycles) and (b) few-cycle (1.4 cycles) laser pulse, at 0.8 μm (red circles), 1.3 μm (green diamonds) and 2.0 μm (purple triangles). In the multi-cycle case (a) the yield increases faster with an increase of the pressure the longer the wavelength of the driving pulse is. We attribute this behavior to the influence of reabsorption of the near-UV harmonics in the helium target. In Fig. 2(e) one can observe how at 0.8 μm wavelength the yield of low-order harmonics is substantially reduced at high pressures. In test calculations we removed the effect of reabsorption in the generating medium from the simulations. The results, presented by dashed lines in Fig. 3(a), confirm that the yield increases when absorption is not taken into account and the increase is largest at the smallest driver wavelength (0.8 μm, red lines with circles).

However, even without absorption the yields do not follow the pressure square rule expected for perfect phase-matching [48]. We have found that this deviation mainly results from the transverse phase mismatch [49], given by $\Delta k_q^\perp = k_q - \frac{\partial \phi_q}{\partial \rho}$, which is not perfect due to the transverse intensity distribution in our focusing geometry. To further support our conclusions, we have performed one-dimensional simulations for a 2 μm driver (yellow line), where transverse phase-matching does not play a role. We observe that the 1D scaling is closer to the pressure-square rule, thus illustrating the relevance of transverse phase-matching in our 3D scenario. On the other hand, the results in Fig. 3(b) show that the integrated yield increase at a lower rate for the few-cycle (1.4 cycles) laser pulses as compared to the multi-cycle cases shown in Fig. 3(a). The difference in the increase between the two cases is strongest for the longest wavelength which clearly shows the highest yields for the multi-cycle pulse. As we will demonstrate below this effect is due to group velocity matching.

The effect of group velocity matching (GVM) in HHG has been studied recently for the first time [50]. Propagation effects have been usually understood in terms of phase velocity matching, however, for media with a high density-length product the group velocity of the harmonics and of the fundamental can differ substantially, as it is well known for perturbative
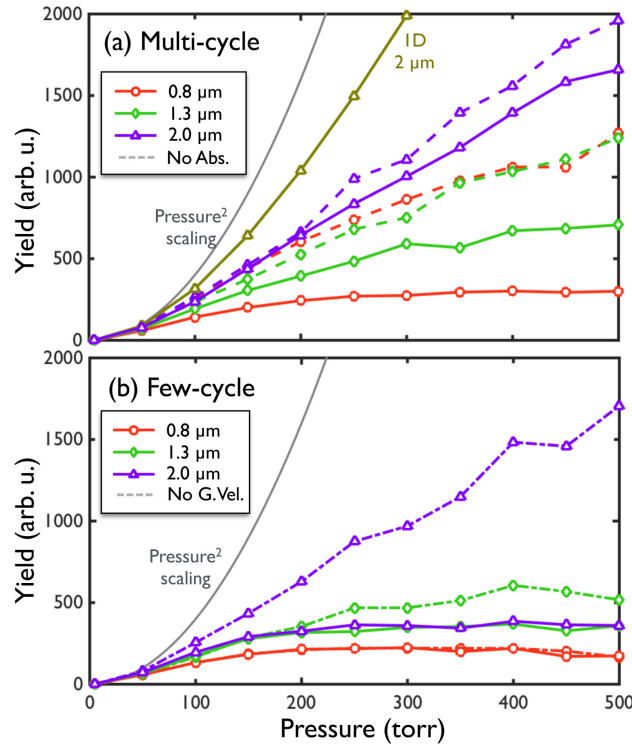
Fig. 3. Influence of group-velocity matching and absorption on the isolated attosecond pulse yields. We show the integrated yield of the central attosecond pulse as a function of gas pressure for a (a) multi-cycle (5.8) and (b) few-cycle (1.4) driving laser pulse of wavelengths 0.8 μm (red circles), 1.3 μm (green diamonds) and 2.0 μm (purple triangles). In panel (a) the dashed lines correspond to the simulations where absorption is not taken into account in the simulations. The yellow line represents the results of one-dimensional simulations at 2 μm for the sake of comparison. In panel (b), the dashed lines correspond to simulations where group velocity mismatch is not considered (absorption included), showing the relevance of group velocity walk off in the case of few-cycle laser pulses.

harmonic generation in crystals [51,52]. Since in the present time-gated technique perfect phase matching is achieved in media with a high pressure-length product, the role of GVM is not longer negligible. The group velocity, given by $v_g(\lambda)^{-1} = n(\lambda)/c - \lambda/c\partial n(\lambda)/\partial\lambda$, imprints a time delay in the envelope of the fundamental laser pulse as it propagates through the medium. To quantify the GVM process in HHG, one can define –analogous to the coherence length– the walk-off length as [50]

$$L_{walk-off} = \frac{t^\pi_{walk-off}}{\left|\Delta v_g^{-1}\right|} \tag{4}$$

where $\Delta v_g^{-1} = v_g(\lambda_0)^{-1} - c^{-1}$, and $t^\pi_{walk-off}$ is the envelope walk-off time needed to dephase a harmonic by π. The variation of the electric field peak strength due to the change in the carrier to envelope phase during propagation affects the semiclassical action, and thus the phase of the high-order harmonics. Analogous to the coherence length, one can interpret the walk-off length as the propagation distance between two atoms whose harmonic emission interfere destructively due to group velocity mismatch. The walk-off length is found to decrease with a decrease of the pulse duration and for an increase of the wavelength. Thus, whereas group velocity matching

does not affect the harmonic emission if driven by short vacuum ultraviolet wavelengths [53], it is expected to play a significant role for longer mid-IR drivers [50]. Actually, the strong reduction of the harmonic yield for few-cycle long wavelength laser pulses in Fig. 3(b) can be unequivocally related to the group-velocity mismatch. This is confirmed by the results of test calculations [dashed lines in Fig. 3(b)] in which we neglected the group velocity effect. Clearly, one sees that in this case for long driving wavelengths the yields increase at a similar rate as for multi-cycle pulses [Fig. 3(a)]. Thus, we can conclude that for the generation of bright isolated attosecond pulses with the time-gated phase matching technique it is preferable to use multi-cycle pulses for which the effect due to group velocity mismatch is negligible.

Experimentally there is another factor which favors bright high-harmonic and attosecond pulse generation using multi-cycle driver wavelengths, related to the optimal pressure-length product to reach the absorption-limited length. The required pressure-length products to reach the maximum HHG yield are much higher for longer driving wavelengths. This is defined as $\sim 6 \times L_{abs}$, where L_{abs} is the absorption-limited length. For example, for He and 0.8, 1.3 and 2 μm drivers the pressure-length products increase significantly from 1.3×10^4, 9.1×10^4, up to 6.1×10^5 torr·mm, for both a gas-cell or a waveguide HHG geometry. As the driving laser wavelength increases towards the mid-IR, the HHG flux reduces even faster for few-cycle laser pulses since the signal buildup starts to decrease at much lower pressure compared to using multi-cycle pulses (see Fig. 1 and Fig. 3). As a result, few-cycle longer-wavelength drivers cannot fully benefit from the allowed very high pressure-length product to compensate for the low single-atom yield.

3.3. Robustness of isolated soft x-ray attosecond pulses against fluctuations

Finally, we proceed to investigate how fluctuations in the electric field of the driving laser pulse may affect the generation of soft x-ray isolated attosecond pulses through the time-gated phase matching technique. The phase matching condition, which is related to the optimal ionized population in the medium, yields an ideal peak intensity for a given wavelength and pulse duration. As a consequence, we may expect that variations of the carrier-envelope-phase (CEP) offset and the peak intensity of the driving laser pulse modify the temporal window for perfect phase matching. Previous studies indicated the robustness against CEP in the generation of XUV attosecond pulses driven by 800 nm laser pulses [19].

In figure 4 we present the yields and temporal profiles of the pulses, generated at 150 Torr with a $\lambda = 2 \ \mu m$, $\tau_p = 5.8$ cycles laser pulse, as functions of (a) the carrier-envelope-phase (ϕ_{CEO}) and (b) the peak intensity. It is seen that the variation of the carrier-envelope-phase and the related change of the temporal window for phase matching, leads, in general, to a change from the emission of a bright isolated attosecond pulse for the optimal $\phi_{CEO} = 0$, at which all the previous analysis has been done, to a two pulse structure, which is strongly suppressed in its yield. More important however, the time-gated phase-matching isolation technique appears to be rather robust for variations over a rather wide range of carrier-envelope-phases, for the present set of simulations from $\phi_{CEO} = -\pi/4$ to $\phi_{CEO} = \pi/4$. For comparison, most of CEP stabilized laser systems have much lower CEP variation on the scale of sub-200 mrad [35,54–56].

On the other hand, an intensity increase will move the phase matching window towards the front part of the laser pulse, whereas an intensity decrease will move it toward the rear part. As a result, in figure 4(b) we observe how the temporal position of the isolated pulse is shifted with intensity, which is being stable within fluctuations of intensity of about ±2.5%, which exceeds the stability of most state-of-the-art laser systems.

4. Conclusions

In summary, we have theoretically analyzed the key parameters for a route to obtain isolated attosecond pulses at high energies, using the time-gated phase matching technique with near-
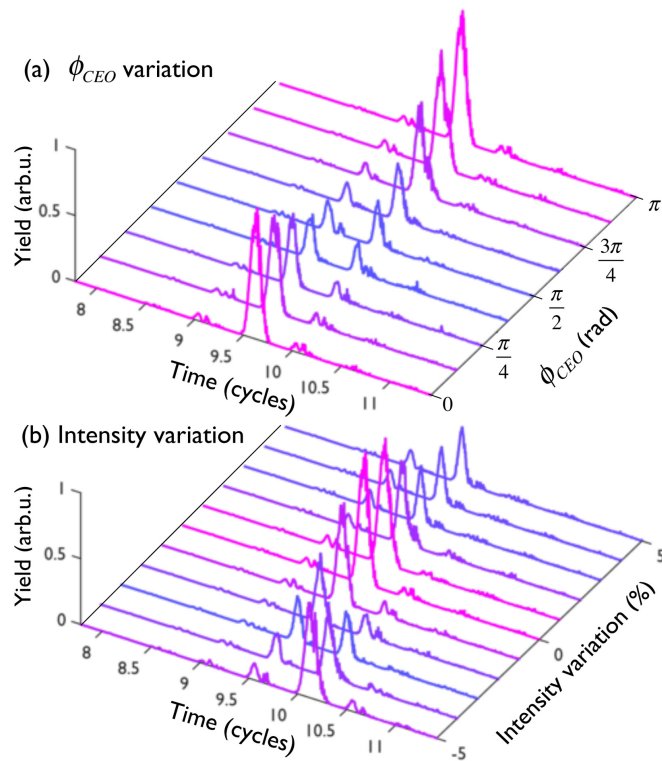
Fig. 4. Robustness of the time-gated phase-matching isolation technique against carrier-envelope-phase and intensity variations. We present the yields and temporal profile of the harmonic emission generated at a gas pressure of 150 Torr with a $\lambda = 2\ \mu m$, $\tau_p = 5.8$ cycles laser pulse, as a function of (a) the carrier-envelope-phase ϕ_{CEO} and (b) the peak intensity of the driving laser pulse. This technique appears to be robust for variations over a rather wide range of carrier-envelope-phases (from $\phi_{CEO} = -\pi/4$ to $\phi_{CEO} = \pi/4$), and within intensity fluctuations of about $\pm 2.5\%$.

and mid-infrared laser pulses. It is shown that the technique allows to generate isolated broad bandwidth harmonic emission at driving laser wavelengths ranging from 0.8 μm to 2 μm. Indeed, the results of the present simulations do not show that there exist a fundamental limitation to apply the technique at even longer wavelengths, which would lead to the generation of isolated attosecond pulse in the keV regime. Our results have further confirmed that the effects of reabsorption and group velocity matching need to be considered and make the technique most effective regarding the brightness of the emission for multi-cycle long driver wavelengths. Finally, our simulations show that the technique is robust with respect to variations of the carrier-envelope-phase and the peak intensity of the laser pulse.

Funding

Acknowledgments